Twin roll casting of Al-Mg alloy with high added impurity content

S. Kumar[1*], N. Hari Babu[2], G.M. Scamans[2], Z. Fan[2], K.A.Q. O'Reilly[1]

[1]Department of Materials, The EPSRC Centre for Innovative Manufacturing in Liquid Metal Engineering, University of Oxford, Parks Road, Oxford, OX1 3PH, United Kingdom.

[2]BCAST, The EPSRC Centre for Innovative Manufacturing in Liquid Metal Engineering, Brunel University, BCAST, Uxbridge, UB8 3PH, United Kingdom.

Abstract

The microstructural evolution during twin roll casting (TRC) and downstream processing of AA5754 Al alloy with high added impurity content have been investigated. Strip casts with a high impurity content resulted in coarse α-Al grains and complex secondary phases. The grain size and centreline segregation reduced significantly on the addition of Al-Ti-B grain refiner (GR). Coarse-dendrite arm spacing (DAS) "floating" grains are observed in the impure alloy (IA) with higher volume in the GR strips. Two dimensional (2D) metallographic analysis of the as-cast strip suggests secondary phases (Fe bearing intermetallics and Mg_2Si) are discrete and located at the α-Al cell/grain boundaries, while three dimensional (3D) analysis of extracted particles revealed that they were intact, well interconnected and located in interdendritic regions. Homogenizing heat treatment of the cast strip breaks the interconnective networks and modifies the secondary phases to more equiaxed morphology. During rolling, the eqiaxed secondary phases align along the rolling direction. X-ray diffraction (XRD) analysis suggests that α-Al(FeMn)Si and Mg_2Si are the predominant secondary phases that formed during casting and remain throughout the downstream processing of the GR-IA. The high

* Corresponding author email id: kumar.sundaram@materials.ox.ac.uk

impurity sheet processed from TRC resulted in superior strength and ductility than the sheet processed from small book mould ingot casting. This study, have shown that the twin roll casting process can tolerate higher impurity levels and produce formable sheets from recycled aluminium for structural applications.

Keywords: TRC; Al-Mg alloys; Recycling; Grain refiner; Intermetallics;

1. Introduction

The increasing need to recycle Al [1] is the driving force for researchers to develop and design new alloys with a wide range of impurities [2] and sustainable low cost casting technologies [3-6]. In our previous studies [7, 8], an alloy containing a high level of impurities was designed based on the composition of a AA5754 alloy from a high level of recycled old rolled aluminium sheet as the postconsumer scrap source. Presence of impurities like Fe, Si and Cu react with other alloy elements during solidification and result in coarse secondary phases in the final ingot microstructure. During rolling deformation these insoluble secondary phases break into fine clusters of particles. But the sheet processed from the high impurity alloy resulted in poor tensile properties and reduced formability compared with that of a purer alloy [7]. Twin roll casting (TRC) is a promising route to producing high quality sheet [9-15]. Recently researchers used TRC to produce sheet with a high impurity constant, specifically focussed on Fe levels [16-18]. In the present study, for the first time we aimed to produce high quality sheet from a very highly impure Al-Mg-Mn-Fe-Cu-Si alloy using twin roll casting.

Since the downstream processing conditions (homogenisation/rolling/extrusion) of the cast strip is dependent on the as-cast grain size and insoluble secondary phases present [7], in this study an attempt was made to reveal the 3D nature of the secondary phases in the TRC strip

and their influence on rolling deformation. A phase extraction technique is used for the first time to facilitate viewing the 3D nature of secondary phases in as-cast and homogenised strip. In this technique, the secondary phases where extracted by dissolving the Al matrix in anhydrous boiling Butan-1-ol. A systematic study was performed to understand the changes in secondary phase nature during casting and subsequent down-stream processing. In-addition, this study also investigates the microstructural evolution during twin roll casting and subsequent downstream processing. The tensile properties of sheets processed from TRC and book mould casting were compared and a cost effective processing route is proposed to produce high strength and good quality formable sheets from highly impure alloys.

2. Experimental Details

The composition of the primary (or pure) AA5754 Al alloy (PA) used in this study is given in Table 1. The primary alloy sheet was re-melted in a clay graphite crucible in a heat resistance furnace at a temperature of 1023.15 K (750 °C). Impurity additions of 0.6 wt % Fe, 0.8 wt % Si, and 0.5 wt % Cu were made to the melt in the form of Al-46 wt % Fe and Al-50 wt % Si master alloys and as pure copper. The final composition of the impure alloy (IA) is also given in Table 1. For further details of the alloy preparation, refer to [7, 8]. For the grain refinement experiments, 0.1 wt% of Al-5Ti-1B grain refiner was added to the liquid metal 10 min before casting. A horizontal twin roll caster with water cooled steel rolls of 100 mm width and 175 mm diameter was used for these experiments. The liquid metal (without and with grain refiner) was poured into a preheated tundish at a melt temperature of 953.15 K (680 °C). The tundish delivers the liquid metal between the two oppositely rotating rolls. The strip with thickness of 5.4 ± 0.24 mm was cast at a rate of 2 m/min. Further details of the twin roll caster setup and experimental procedures can be found in ref [14, 18]. The cast strip was later homogenised (H) at 833.15 K (560 °C) with a heating and cooling ramp rate of 303.15 K (30 °C) per hr. The

homogenised strip was cold rolled to 1 mm thin sheet (after 20 pass). Rolled sheets were solution heat treated (SHT), i.e. annealed at 530 °C for 60 sec in a salt bath followed by water quenching.

The tensile tests were performed on 220-mm-long, full-sized specimens with an extensometer on the 50-mm gage length, according to ASTM E8M-08 standard. The tensile properties of the annealed sheets were measured along the rolling direction. The three dimensional (3D) analysis was carried out on the extracted intermetallic particles. Anhydrous boiling Butan1ol was used to dissolve the Al matrix and a poly-tetrafluoroethene (PTFE) filter membrane (47 mm diameter, pore size of 0.2 μm) was used to collect the intermetallic particles. Two dimensional (2D) microstructural analyses were carried out on longitudinal (L) and transverse (T) cross-sections. Samples were mounted and ground and then polished with colloidal silica suspension with a particle size of 0.04 μm. As-polished samples were used to examine segregation and the morphology and distribution of the intermetallic phases. In-order to measure the grain size, polished samples were anodized at 20 V for 60 seconds in Barker's reagent (7 ml HBF_4 (48 pct), 93 ml H_2O). The linear intercept method was used to measure the grain size on polarized images taken with a Zeiss Axioskop 2 MAT optical microscope (Carl Zeiss, Hertford Shire, UK). A Zeiss EVO 50 scanning electron microscope (SEM, Carl Zeiss NTS GmbH, Oberkochen, Germany) equipped with a Princeton Gamma Tech energy-dispersive spectrometer (EDS, Princeton Gamma-Tech (PGT), Princeton, NJ, USA) was used to image microstructures and analyse the segregation. A field emission gun (FEG) scanning electron microscope (JEOL 840F) was used for 3D analysis of extracted intermetallics. The phases were identified using a Philips 1700 X-ray diffractometer (XRD) with a Cu-K_α (λ = 1.54 A) source at 35KV, 50 mA and 0.05º step size.

3. Results

3.1 Twin roll casting

3.1.1 Grain size and dendritic arm spacing (DAS)

Figure 1 and Figure 2 shows the anodised microstructures and average grain size of the as-cast TRC strips. The IA strip has a coarser grain size than the PA. The variation in grain size between L and T cross-sections is due to elongated grains as the result of heat extraction and subsequent deformation during solidification between the two rolls. The addition of grain refiner reduces the grain size significantly in both alloy strips. Specifically the coarse grains in IA have changed into fine grains after addition of grain refiner. Though the anodized microstructure shows relatively uniform grain size across the cross-section of the IA strips, it is interesting to observe the presence of a few grains with coarse DAS (Fig. 3) known as "floating" grains. Such grains were observed in larger proportion (~58 grains/mm^2) in the GR added IA strips (Fig. 3b) when compared to non-grain refined IA strips (~13 grains/mm^2). Table 2 clearly shows the DAS of different grains observed in the as-cast strip of IA with and without GR. The DAS of coarser DAS grains were larger for the non-grain refined IA strip.

3.1.2 Centreline-segregation

The strip cast from IA (Fig. 4a) resulted in severe centreline segregation. A magnified image of the centreline segregation (Fig. 5) shows the presence of various eutectic phases with complex morphologies. The observation of star shaped Fe bearing intermetallic particles (Fig. 5a) at the strip centre suggests that the region solidified from a liquid rich in Fe. More frequently, ternary eutectic (Fig. 5b) consisting of Al, Mg-Si rich phase and Fe bearing intermetallic was observed at both interdendritic and centreline segregated regions of the strip, but no such ternary eutectic was observed in the book mould cast ingots [7, 8]. Similarly, α-Al and Mg-Si lamella eutectic (Fig. 5c) was also observed. In addition, a large volume of fine

eutectic lamella of α-Al and Cu-Al (Fig. 5d) was observed in the centre-line segregation which suggests that Cu and Mg segregate severely at the centre of the strip in addition to Fe. Mg segregation at the strip centre was observed in the TRC strips of Al-Mg alloys [18]. Interestingly, the GR added IA strip has no such severe centreline segregation (Fig. 4b) and this is attributed to (a) different sump profile and (b) fine grain size. Similar absence of centre line segregation with the addition of Al-Ti-B grain refiner was reported by Birol [19].

3.1.3 Secondary phases

A) Two dimensional (2D) analysis

2D analysis of metallographic samples of the IA+GR strips shows fine and discrete secondary phases distributed at cell/grain boundaries (Fig. 4b). High magnification images show the presence of fine binary and ternary lamella eutectics (similar to Fig. 5b,c). Interestingly when IA with grain refiner addition was cast as a book mould ingot there were no such lamella eutectics observed, instead coarser platelet-type and Chinese script-type Fe bearing intermetallic particles were observed [7, 8]. Elemental mapping along the interdendritic region (Fig. 6) shows that the region is rich in Mg, Fe and Cu. This suggests that micro segregation of solute elements to the interdendritic regions influences the formation of different intermetallics.

B) Three dimensional (3D) analysis

In-order to understand the nature of the Fe bearing intermetallic particles and other secondary phases that form during the solidification in TRC, the Al matrix was dissolved and the remaining extracted particles were analysed in 3D. After dissolving the matrix a free-standing, fine-pored foam-like structure was observed comprising an interconnected particle network (Fig. 7a). Each pore is ~5 μm in size (arrow mark in Fig. 7b) which typically represents the size of the dendrite arm spacing of α-Al in the GR IA strip. The intermetallics had a surprising

and previously under-appreciated ability to adopt curved and convoluted morphologies around dendrites. Further microscopical analysis showed that these intermetallics are well interconnected, intact, inter-dendritic and had a fibre-like morphology (Fig. 7c) with thickness and spacing of 130 and 275 nm respectively. XRD analysis (Fig. 8a) of the extracted particles of as-cast strip, (IA+GR), confirms that α-Al(FeMn)Si and Mg_2Si are the predominant secondary phases.

3.2 Homogenisation

Figure 9 shows the homogenised microstructure of the IA+GR strip. Interestingly, only equiaxed particles of secondary phases were observed in the homogenised metallographic sample (Fig. 9a) and no dendritic-type coupled eutectics, as in the as-cast strip (Fig. 5). The 3D analysis further revealed that the interconnected network of intermetallics observed in the as-cast strip was broken down into fine particles during homogenisation (Fig. 9b). In addition, these particles had two distinct size distributions. EDS analysis on the extracted sample suggested that the large particles were rich in Mg and Si whereas the small particles were rich in Fe. The 3D analysis further revealed that Mg and Si rich particles in the homogenised strip were octahedral in shape (Fig. 9c) and not spherical as observed in 2D analysis, whereas Fe bearing particles were spherical (Fig. 9d). XRD analysis (Fig. 8b) of the extracted particles from the homogenised strip, (IA+GR+H), confirms the presence of only α-Al(FeMn)Si and Mg_2Si.

3.3 Rolling and solution heat treatment

During rolling, these intermetallic particle clusters further break-up and align along the rolling direction (Fig. 10a). Higher magnification (Fig. 10b) shows the presence of fine, apparently discrete Fe bearing intermetallics and Mg_2Si particles. The 3D analysis clearly shows that the

secondary phase particles in the sheet processed from TRC (Fig. 11b) are finer (average particle size 0.5 μm) than those found in the sheet processed from book mould casting (average particle size 5.5 μm) (Fig. 11a). Further analysis of the particles extracted from the TRC processed sheet showed that the Fe bearing intermetallics are finer (160 nm) than the Mg_2Si particles (1 μm) (Fig. 11c). In most cases, the Fe bearing particles are in the form of fine clusters (500 nm). XRD analysis (Fig. 8c) of the extracted particles of the solution heat treated sheet (IA+GR+SHT) also confirms only the presence of α-Al(FeMn)Si and Mg_2Si. But it is interesting to note that the relative peak intensity ratio of the Fe bearing intermetallics and Mg_2Si increased in the SHT sheet when compared to that observed in homogenised strip. The grain size in the solution heat-treated sheet (Fig 12) is 17 ± 6 μm which is similar to that in the book mould processed sheet.

3.4 Tensile test comparison

The true stress-strain curves of the IA+GR sheets processed from TRC and book mould casting are shown in Fig. 13. The properties presented were measured along the rolling direction. The sheet processed from the TRC resulted in 5% decrease in yield strength, 10 % increase in ultimate tensile strength (UTS) and 40% increase in elongation when compared to the sheet processed from book mould ingot casting (Table 3).

4. Discussions

4.1 Microstructure evolution during casting

4.1.1 Grain size

In general, during solidification in the TRC process, dendrites form from the surface of the water cooled steel rolls and grow in the opposite direction to that of the heat extraction i.e. away from the roll surface. During the growth of dendrites, solute elements segregate at the

solid-liquid interface and provide sufficient constitutional under-cooling for further nucleation of α-Al and the process continues until the two opposite growing interfaces merge. Thus the L and T cross-sections reveal different grain orientations and grain size variations as observed (Fig. 2). It is important to mention here that the source metal used in this study was post-consumer rolled sheet scrap, which had previously been grain refined and processed, and hence should contain some nucleating substrates (TiB$_2$) and excess solute Ti for growth restriction. Therefore the observed increase in grain size (Fig. 1 and Fig. 2) on the addition of impurities (Fe, Si and Cu) could be explained through (a) nucleation criteria and (b) growth restriction criteria. From the nucleation view point, this can happen if the nucleating potency of pre-existing substrates such as TiB$_2$ was reduced either by (a) formation of complex intermetallic compounds over the surface of the TiB$_2$ or (b) a change in substrate/liquid interfacial energy as a result of changes in overall chemical composition. Analysis of the nature of particles existing in the impure alloy liquid metal, before casting, using the pressure infiltration technique confirmed the presence of complex compounds on the Ti rich particles [8]. Thus the formation of complex compounds on the nucleants and their clustering reduces their potency and efficiency, which is one of the reasons for the increase in grain size observed in the IA strips (Figs. 1 and 2). Difference in grain size between these two alloys was observed even in book mould ingot casting [8].

From the growth restriction view point, one would expect that the addition of solute elements such as Fe, Si and Cu, would increase both the growth restriction parameter (Q) and undercooling parameter (P). Q and P can be empirically defined as $Q = \sum_{i=1}^{N} m_i C_0 (k_i - 1)$ and $P = \sum_{i=1}^{N} m_i C_0 (k_i - 1) / k_i$, where C_0 is the elemental composition, m is the liquidus slope of the binary alloy, k is the equilibrium partition coefficient, N is the total number of solute elements, and i denotes the ith element in the bulk composition [20, 21]. Using the above

9

empirical equations, Q for PA and IA composition (Si, Fe, Mg, Mn and Cu elements only used) were calculated as 10 and 16, and P for PA and IA composition are calculated as 41 and 114. Such increase in Q and P should reduce the grain size [20], but this is not the case in the present study where the grain size increased on the addition of solutes. Generally in dilute Al alloy systems, once the primary Al nucleates, the dendrite starts to grow, and the solute element with the highest k segregates at the growing solid-liquid interface. Thus the segregated solute slows the growth of the dendrite and provides sufficient under-cooling for nearby potent substrates to nucleate, so resulting in a finer grain size [20]. In the present case, the observed increase in grain size (Fig. 1 and Fig. 2) is because the impure alloy is heavily prone to forming various intermetallic compounds from liquid during solidification (discussed in section 4.3), which consumes large amount of segregated solutes such as Si, Mg, Fe and Cu, while less remain for growth restriction contribution. In addition, there might be loss of Ti, which has a high k, by forming complex intermetallics [7] at a temperature higher than the Al liquidus temperature, and thus leaving less solute Ti available for growth restriction during solidification.

It is important to note that in a binary Al alloy, both Q and P are proportional to the equilibrium solidification range or interval ($\Delta T = T_L - T_S$), i.e. $\Delta T = P = Q / k$, where T_L is the liquidus temperature and T_S is the solidus temperature [21]. In many hypoeutectic binary Al alloys, the grain size increases up to a maximum ΔT where solid solubility of solute is a maximum and any further increases in solute increase the grain size [22, 23]. According to thermodynamic calculation using MTDATA studio 5.10 with NPL aluminium database V6.1, version, the ΔT for PA and IA were ~ 36 K and 48 K, respectively. Hence IA which has a higher ΔT is expected to have fine grains according to the solidification interval theory, but this is definitely not the case in the multicomponent system as in the present study. Similar behaviour has been observed in the Al-Mg binary alloy system, where the grain size decreased upto the eutectic composition

rather than to a maximum solidification interval [24]. It is evident that the solidification interval of an alloy varies with respect to solidification conditions [25]. Based on this an attempt was made to correlate grain size with ΔT using a Scheil calculation, which resulted in good agreement with the grain size differences as observed in the present case i.e. the alloy having the larger solidification interval calculated by Scheil (PA~205 K) resulted in a finer grain size than the alloy with smaller (IA~195 K) solidification interval. It is interesting to note that the addition of excessive grain refiner reduces the grain size of IA significantly. This is due to providing excessive TiB2 and Ti solute in the form of grain refiner addition. In all cases, the grain refiner addition resulted in finer Al grain size.

4.1.2 Dendrite arm spacing

As TRC provides a higher cooling rate (10^3 K/s) [26], the morphology of primary Al grains in the as-cast strips are observed to be heavily dendritic irrespective of addition of Al-Ti-B grain refiner or impurity elements. The DAS of the IA strips are much finer than those usually observed in book mould ingots [7, 8]. Surprisingly, there were also a few coarser DAS (foreign) grains observed along with fine DAS (native) grains near the strip surface (examples of coarser DAS grains are indicated in Fig. 3). Such coarse DAS grains would have nucleated and grown early on in the solidification and been transported to this location before being trapped by native grains. The mechanism of formation of such grains can be explained using the illustration shown in Fig. 14. The solidification regime (also known as the sump) in the TRC process can be classified into (a) liquid, (b) semi-solid and (c) solid regions. The semi-solid region can be further divided into (d) slurry and (e) mushy zone. The region where the primary Al nucleates and grows is called the slurry zone (Z1) and the region where the dendrites collide and coarsening starts is called the mushy zone (Z2). Liquid flow in TRC is inevitable, therefore any flow of liquid near the slurry zone may transport pre-nucleated crystals from Z1 to other parts

of the casting (thus known as "floating" grains). During this transportation, the DAS of these floating grains coarsens. At some stage these coarse DAS floating grains get trapped at the growing solid-liquid interface and thus result in a dual DAS grain structure, as observed in Fig 3. In some cases, those trapped coarse DAS "floating" grains further grow in the remaining liquid with fine DAS (DAS similar to native grains) as the result of different solidification condition. It is interesting to note that the number of the coarse DAS "floating" grains is 4 times larger in the grain refiner added strip (Fig. 3b). This can be explained based on the changes in the solidification sump profile. Usually the addition of grain refiner reduces the coherency temperature (coherency temperature is the temperature at a point of an alloy where individual dendrites first impinge upon their neighbours during solidification) and increases the permeability of the mushy zone (Z2) [27]. Therefore grain refiner addition widens the slurry zone (Z1) by increasing the number density of nucleated crystals and reduces the mushy zone (Z2) by reducing the coherency temperature. Thus a large volume of nucleated crystals in Z1 can be easily transported by the liquid flow in GR added alloys and hence a large number of coarse DAS grains was observed in the final microstructure of the GR added strip (Fig. 3b). Similar coarse DAS grains in TRC strip have been observed by Yang [28] and Strid [29]. Strid [29] proposed that floating grains can also form if the solidification front is located between the feed tip and the metal-roll contact point.

4.1.3 Centreline segregation

Formation of centreline segregation can also be explained using the illustration shown in Fig. 14. During solidification in the TRC process, the two opposite growing solid-liquid interfaces result in enrichment of the liquid towards the sump centre. When this part of the mushy zone experiences the rollers load, the solute rich cooler liquid squeezes out parallel to the cast direction. Thus the flow of solute rich liquid can dissolves relatively solute poor dendrites,

results in the formation of channels. These channels fill back with hot liquid again. With further casting motion, at some stage, liquid inside the channel gets trapped when both of the solid surfaces get welded together under load. Thus this trapped liquid experiences high cooling rate and results in fine eutectic structures as observed (Fig. 4 and 5). This clearly explains the present observation of severe segregation in the alloy strip without grain refiner addition (Fig. 4(a)). However this effect is less pronounced in the alloy with grain refiner, due to changes in the sump profile. The presence of potent nucleating substrates helps in nucleating a large number density of α-Al crystals which inherently increases the size of the slurry zone. As stated earlier, addition of GR increases the permeability and reduces the coherency temperature in the mushy zone [21]. In other word, the size of the mushy zone is reduced with addition of GR. It has also been observed that the depth of the sump varies with alloy composition [20]. In addition, during solidification the excessive solute elements (above α-Al solid solubility) segregate along the cell or grain boundaries. Thus the larger grain boundary area in the grain refined alloy accommodates more solute rich liquid and results in less solute segregation at the centre of the strip. Hence the combination of change in sump profile and solute segregation reduces the probability of the mushy zone experiencing the roller load and this result in reduced centreline segregation (Fig. 4(b)) in GR added alloy.

4.1.4 Secondary phases

The solid solubility of Fe and Si in Al varies and is dependent on the presence of other solute elements and solidification conditions. During solidification of this Al-Mg alloy the excessive solute elements segregate to the liquid at the solid-liquid interfaces. As the temperature drops, various secondary phases form from the solute rich liquid as the result of different variant and invariant reactions. Thermodynamic simulations under Scheil conditions for the impure alloy (Fig. 15) suggest the formation of a sequence of secondary phases as the temperature drops

normally: $Al_6Mn(Fe)$, $Al_{13}Fe_4$, Mg_2Si, S-phase (Al_2CuMg) and Q-phase (AlMgSiCu). But the XRD analysis (Fig. 8) of the extracted particles from the as-cast IA strip suggests the presence of only α-Al(FeMn)Si and Mg_2Si. This is because TRC is a non-equilibrium solidification process, where the cooling rate reaches upto 10^3 K/s, resulting in different solute segregation levels in the interdendritic liquid and thus different secondary phases form to those predicted. This also explains the observation of predominant Si rich secondary phases (α-Al(FeMn)Si and Mg_2Si) in the as-cast strip, because there is less time for Si to diffusion back from the solute rich liquid to the α-Al under such high solidification rates [30]. The absence of Al_2CuMg and AlMgSiCu phases in the XRD analysis is attributed to them being present in a volume fraction below the detection limit.

It is interesting to note that though the 2D analysis suggests the secondary phases were fine and discrete, the 3D analysis revealed that these secondary phases were well intact, interconnected and in a continuous network. It is important to note that this true nature of the secondary phases cannot be revealed by 2D metallographic analysis and in most cases is misinterpreted. These secondary phase particles were formed in the interdendritic region of the primary Al and are well interconnected (Fig. 7). It has been previously observed that the interconnectivity depends on cooling rate; the higher the cooling rate the thinner/weaker the interconnection [31]. However in the present case, though the cooling rate is much higher than previous work [31], the secondary phases are well interconnected. This further suggests that the initial alloy composition plays a significant role in the interconnectivity, in addition to the cooling rate. The 3D morphological analysis of the secondary phases of the IA strip suggest that the interconnected network is made of fine, long fibre-like, regularly spaced intermetallic particles. The pore size of the secondary phase is dictated by dendrite arm spacing. It is also

important to note that though the strip underwent deformation after solidification during the TRC process, the intermetallics are still well interconnected and intact.

4.2 Microstructural evolution during down-stream processing

It is important to note that the as-cast GR-IA strip was severely cracked when cold rolled (Fig. 16). One reasons for this could be that dislocations generated in the Al matrix during rolling deformation, may pile-up at the interdendritic regions where the highly interconnected brittle secondary phase (Fe bearing and Mg_2Si) network is observed. When the local stress reaches the fracture strength of the secondary phases a crack initiates and propagates throughout the cross-section and results in strip fracture. After homogenisation, the strips were successfully cold rolled to 1 mm thick sheet (Fig. 10). In addition, Mg is one of the primary strengthening elements in Al-Mg alloys, hence severe segregation of this element to the interdendrite regions (Fig 6) will result in poor performance of the components. Therefore this alloy strip needs to undergo a homogenisation process for successful rolling into thin strips.

Homogenisation resulted in (a) breaking of the highly interconnected intermetallic networks into fine clusters of particles (Fig. 9), (b) spheriodization of the Fe bearing intermetallics and Mg_2Si particles and (c) reduce solute concentration gradients within the α-Al. Since Mg_2Si forms as an equilibrium phase from the liquid during solidification for this alloy composition, homogenisation does not dissolve these particles back into solid solution, rather they tend to spheriodiced in-order to reduce their surface energy. It is interesting to note that most of the large equi-axed Mg_2Si particles were observed at the triple junctions of the cell or grain boundaries. This is due to dissolution of fine particles and growth of larger particles particularly in a place where solute elements can easily be transported, such as grain boundary triple junctions (as observed). Since the homogenisation temperature for this alloy is below the

15

melting temperature of Mg_2Si, the dissolution of Mg_2Si in this case is probably due to solute diffusion i.e. either volume (α-Al crystal lattice) or grain boundary diffusion. Usta *et al* [32], suggested that coarsening of Mg_2Si is diffusion controlled with grain-boundary diffusion dominating volume diffusion. Similarly, Fe bearing intermetallics which have a fibre-like morphology in the as-cast strips transform into fine necklace structures during homogenisation.

The 3D analysis of the extracted particles in the homogenised strip suggests that Mg_2Si particles are not spherical, rather they have a truncated octahedral-like or rod-like morphologies. Most of the Fe bearing particles were fine and spherical. This supports the idea that Mg_2Si coarsens much faster than the Fe bearing intermetallic under this homogenisation practice. Though there were changes in the morphology and interconnectivity of the secondary phases, the type of phases seems to remain the same during casting and homogenisation. But there is a slight change in the relative proportion of Mg_2Si and α-Al(FeMn)Si in the sheet processed after rolling compared with after solution heat treatment. This can be explained based on dissolution induced by deformation [33, 34]. Rolling induces a large density of dislocation in the homogenised strip and thus promotes further dissolution of Mg_2Si into the primary Al during SHT and so reduces its relative fraction. During cold rolling, both the Fe bearing intermetallics and Mg_2Si particle clusters break up further (Fig 11c) and align along the rolling direction (Fig. 10).

4.3. *Comparison between TRC and Book mould processed sheets*

TRC processed IA sheet resulted in improved tensile properties (present study) compared with those of book mould ingot processed sheet (previous study). This is attributed to the presence of fine secondary phase particles and its fine clusters in the TRC processed final sheet. Due to high cooling rate, solidification in TRC resulted in an as-cast microstructure with a fine Fe

bearing intermetallic and Mg_2Si network. These fine secondary phases spheroidse during homogenisation and they align along the rolling direction during rolling deformation. In the book mould casting due to a slower cooling rate, the as-cast microstructure results in coarse complex-shaped Fe bearing intermetallics and Mg_2Si particles [7, 8]. Only part of the secondary phase spheroidise during ingot homogenisation and the remaining complex shaped in-soluble particles break into clusters of particles during rolling, which leads to them aligning along the rolling direction [7]. When these sheets are subjected to tensile loading, the coarse particles in the clusters act as nucleation sites for voids to form and results in fracture at lower loads [7]. Figure 11 shows that book mould ingot processed sheet has coarser secondary phase particles. Thus the presence of coarse clusters of coarse-sized secondary phase particles in the sheet processed from the book mould ingot resulted in poor strength and ductility. It has been reported that there is a difference in crystallographic texture between sheets processed from TRC and DC casting, with the latter having a stronger cubic texture [10]. From the present observations it seems that the size and distribution of constituent particles also plays a significant role in determining the final sheet properties, specifically when there is a large volume of coarse secondary phase particles. Therefore to have high quality components from highly impure alloys, it is essential to have fine secondary phase particles in the final product. Hence it is important to control the nature of secondary phases forming during the solidification process. Thus, the TRC process seems to be a promising route to produce sheets from high impurity scrap metal.

5. Conclusions

Twin roll casting of 5754 Al alloy with deliberate addition of Fe, Si and Cu modifies the distribution of intermetallic particles in the as-cast strip and this results in improved fracture properties of sheet produced after thermo-mechanically processing the strip. Addition of grain

refiner reduces the grain size and centreline segregation but increases the volume of coarse DAS "floating" grains. The 3D analysis of extracted intermetallics plays a critical role in understanding the factors controlling the Fe bearing intermetallic morphology and interconnectivity. While 2D sections show intermetallic phase size and shape after casting and through downstream processing to be expected, they completely failed to reveal the highly interconnected and extended nature of the intermetallics demonstrated in 3D. The intermetallics had a surprising and previously under-appreciated ability to adopt curved and convoluted morphologies around dendrites, which has a dramatic effect on mechanical properties. α-Al(FeMn)Si and Mg_2Si where the predominant secondary phases observed during casting and downstream processing. Twin roll casting can be used to increase the tolerance of Al-Mg alloys to impurities typical of those that accumulate from the use of post-consumer scrap in the melt formulation.

Acknowledgement

References

[1]   G. Rombach: *Acta Mater., 2013,* vol. 61, pp. 1012-20.

[2]   S.K. Das: *Aluminium Alloys 2006, Pts 1 and 2, 2006,* vol. 519-521, pp. 1239-44.

[3]   O. Umezawa, M. Nakamoto, Y. Osawa, K. Suzuki, and S. Kumai: *Mater. Trans.,* 2005, vol. 46, pp. 2609-15.

[4]   X. Fang, G. Shao, Y.Q. Liu, and Z. Fan: *Mater. Sci. Eng.*, 2007, vol. 445, pp. 65-72.

[5]   Y. Osawa, S. Takarnori, T. Kimura, K. Minagawa, and H. Kakisawa: *Mater. Trans.,* 2007, vol. 48, pp. 2467-75.

[6]   P. Mikolajczak and L. Ratke: *3rd International Conference on Advances in Solidification Processes,* vol. 27, 2012.

[7]   S. Kumar, N.H. Babu, G.M. Scamans, and Z. Fan: *Metall. Mater. Trans. A*, 2011, vol. 42A, pp. 3141-49.

[8]   S. Kumar, N.H. Babu, G.M. Scamans, D.G. Eskin, and Z. Fan: *Int. J. Mat. Res.,* 2012, vol. 103, pp. 1228-34.

[9]   X.M. Cheng and J.G. Morris: *Mater. Sci. Eng.*, 2002, vol. 323A, pp. 32-41.

[10]   M. Slamova, M. Karlik, F. Robaut, P. Slama, and M. Veron: *Mater. Charact.,* 2002, vol. 49, pp. 231-40.

[11]   C. Gras, M. Meredith, and J.D. Hunt: *J. Mater. Process. Technol.,* 2005, vol. 169, pp. 156-63.

[12]   Y. Birol: *Mater. Sci. Technol.,* 2006, vol. 22, pp. 987-94.

[13]   S. Das, N.S. Lim, J.B. Seol, H.W. Kim, and C.G. Park: *Mater. Des.,* 2010, vol. 31, pp. 1633-38.

[14]   S. Kumar, N. Hari-Babu, G.M. Scamans, and Z. Fan: in *12th ICAA*, Yokohama, Japan, 2010, pp. 721-26.

[15]   M. Karlik, T. Manik, and H. Lauschmann: *J. Alloys Compd.,* 2012, vol. 515, pp. 108-13.

[16]   T. Haga, M. Ikawa, H. Watari, K. Suzuki, and S. Kumai: *Mater. Trans.,* 2005, vol. 46, pp. 2596-01.

[17]   K. Komeda, T. Haga, and S. Kumai: *Mater. Process. Technol., Pts 1 and 2,* 2011, vol. 154-155, pp. 1544-48.

[18]   S. Kumar, N.H. Babu, G.M. Scamans, and Z. Fan: *Mater. Sci. Technol.,* 2011, vol. 27, pp. 1833-39.

[19]   Y. Birol: *J. Alloys Compd.,* 2007, vol. 430, pp. 179-87.

[20]   M. Easton and D. Stjohn: *Metall. Mater. Trans. A*, 1999*,* vol. 30, pp. 1613-23.

[21]   D.G. Eskin, *Physical metallurgy of direct chill casting of aluminum alloys*. Boca Raton: CRC Press/Taylor & Francis, 2008.

[22]   H. Xu, L.D. Xu, S.J. Zhang, and Q. Han: *Scripta Mater.,* 2006, vol. 54, pp. 2191-96.

[23]   Y. Birol: *Int. J. Mat. Res.,*2013, vol. 26, pp. 22-27.

[24]   Y. Birol: *Mater. Sci. Technol.,* 2012, vol. 28, pp. 924-27.

[25]   Y. Birol: *J. Alloys Compd.,*2009, vol. 486, pp. 168-72.

[26]   M. Ferry, *Direct Strip Casting of Metals and Alloys,* 2006.

[27]   D. G. Eskin, R. Nadella, and L. Katgerman: *Acta Mater.,* 2008, vol. 56, pp. 1358-65.

[28]   X. Yang: PhD, Department of Materials, University of Oxford, Oxford, 1993.

[29]   J. Strid, T. Furu, R. Orsund, and E. Nes: in *Continuous Casting of Non-ferrous Metals and Alloys*, 1989, pp. 119 - 52.

[30]   Y. Langsrud: Balatonfured, Hung, 1990, pp. 95-15.

[31]   A. Verma, S. Kumar, P.S. Grant, and K.A.Q. O'Reilly: *J. Alloys Compd.,* 2013, vol. 555, pp. 274-82.

[32]   M. Usta, M.E. Glicksman, and R.N. Wright: *Metall. Mater. Trans. A,* 2004, vol. 35, pp. 435-38.

[33]   M. Murayama, Z. Horita, and K. Hono: *Acta Mater.,* 2001, vol. 49, pp. 21-29.

[34]   K. Venkateswarlu, M. Chakraborty, and B.S. Murty: *Mater. Sci. Eng.*, 2004, vol. 364A, pp. 75-83.

Figure Captions

Fig. 1 Anodized microstructure of the as-cast TRC strips, (a) PA, (b) IA, (c) PA+GR and (b) IA+GR alloys. The grain size is finer and more uniform in the grain refiner added alloys. The arrows show the cast direction.

Fig. 2 Average grain sizes in the as-cast strips. The addition of grain refiner reduces the grain size.

Fig. 3 Darkfield light microscope images of the anodized LD cross-sectioned (a) IA and (b) IA+GR as-cast TRC strips. The number of coarse dendritic "floating" grains is 4 times higher in the GR strip. DAS is also finer in GR strip. Arrows indicates examples of "floating" grains. Note: inter-dendritic region are brighter in the darkfield reflected-light image.

Fig. 4 Back scattered (BSE) SEM images of the longitudinal direction cross-sectioned (a) IA and (b) IA+GR as-cast TRC strips. Severe centre-line segregation is observed in the strip without grain refiner. Horizontal arrow shows the cast direction.

Fig. 5 High magnification BSE SEM images showing the presence of different phases at the centre-line segregation region of the IA strip cast without grain refiner. Where (a) shows the Fe bearing intermetallic, (b) ternary eutectic of α-Al, Mg_2Si and Fe bearing intermetallic, (c) lamella eutectic of α-Al and Mg_2Si, and (d) lamella eutectic of α-Al and Al-Cu-Mg phase.

Fig. 6 Line scan (EDS) showing microsegregation of solute elements in the inter-dendritic regions.

Fig. 7 3D analysis of the IA+GR as-cast TRC strip. Secondary phase particles are well interconnected (a), and the trace diagram (b) from (a) indicating connectivity which

was used to measure the approximate pore size (arrow). Most of these particles are fibrous in nature (c), with a spacing less than 100 nm.

Fig. 8 XRD patterns of the extracted particles. Corresponding JCPDF file numbers used for indexing are also shown.

Fig. 9 2D and 3D analysis of the homogenised IA+GR TRC strip. The transverse cross-section of homogenised strip (a) shows the cell/grain boundaries decorated with fine Fe bearing intermetallic (bright) and Mg_2Si (dark) particles. Coarse Mg_2Si (marked with arrow) was mainly observed at the triple junctions of the boundaries. 3D analysis of the extracted particles revealed (i) the absence of a dense interconnected network (b), (ii) the equiaxed Mg_2Si particles were facetted (c) and (iii) the equiaxed Fe bearing intermetallics were finer than the Mg_2Si (d).

Fig. 10 BSE-SEM image of the rolled and solutionised sheet, (a) showing intermetallics aligned along the rolling direction, and (b) higher magnification of the Fe bearing intermetallics (bright particles) and Mg_2Si (dark particles). Fe bearing intermetallics are finer than the Mg_2Si.

Fig. 11 FEG-SEM analysis of the extracted particles from the IA+GR sheets processed from (a) book mould ingot and (b,c) TRC stip. Secondary phase particles are finer in the TRC processed sheet.

Fig. 12 Anodized microstructure of the TRC processed sheet after homogenisation, cold rolling and solution treatment.

Fig. 13 True stress-strain curve of the sheets processed from TRC and book mould ingot casting. TRC processed sheet shows superior strength and ductility.

Fig. 14 Schematic illustration of solidification and deformation processes during TRC, where Z1 and Z2 are the slurry and mushy zones, respectively.

Fig. 15 Thermodynamic calculation of phase content in IA, under Scheil condition.

Fig. 16 Light microscopy image taken along the longitudinal cross-section of IA+GR TRC strip

showing that fracture occurred while rolling the as-cast strip without homogenisation.

Figure 1
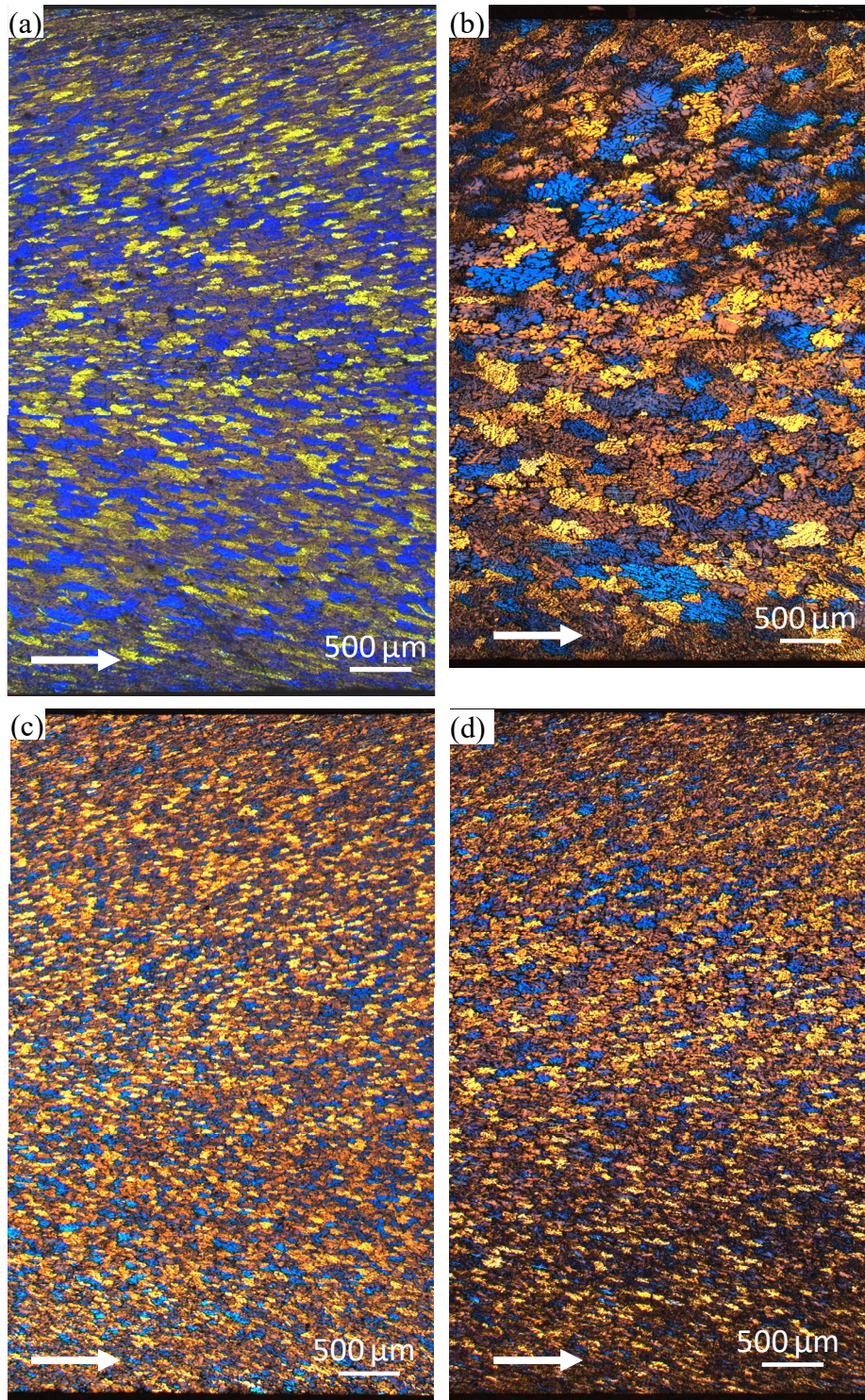
Fig. 1. Anodized microstructure of the as-cast TRC strips, (a) PA, (b) IA, (c) PA+GR and (b) IA+GR alloys. The grain size is finer and more uniform in the grain refiner added alloys. The arrows show the cast direction.
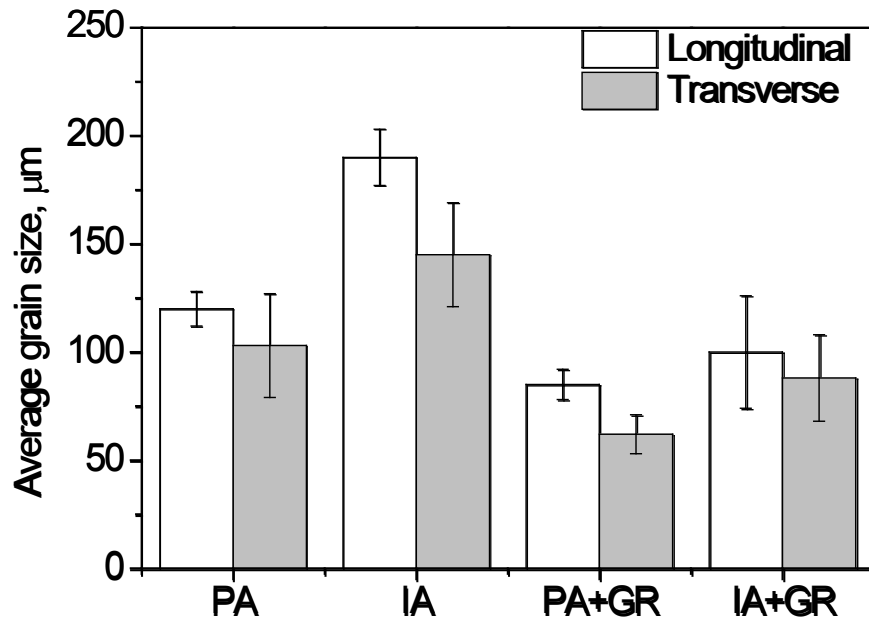
Figure 2

Fig. 2. Average grain sizes in the as-cast strips. The addition of grain refiner reduces the grain size.

Figure 3
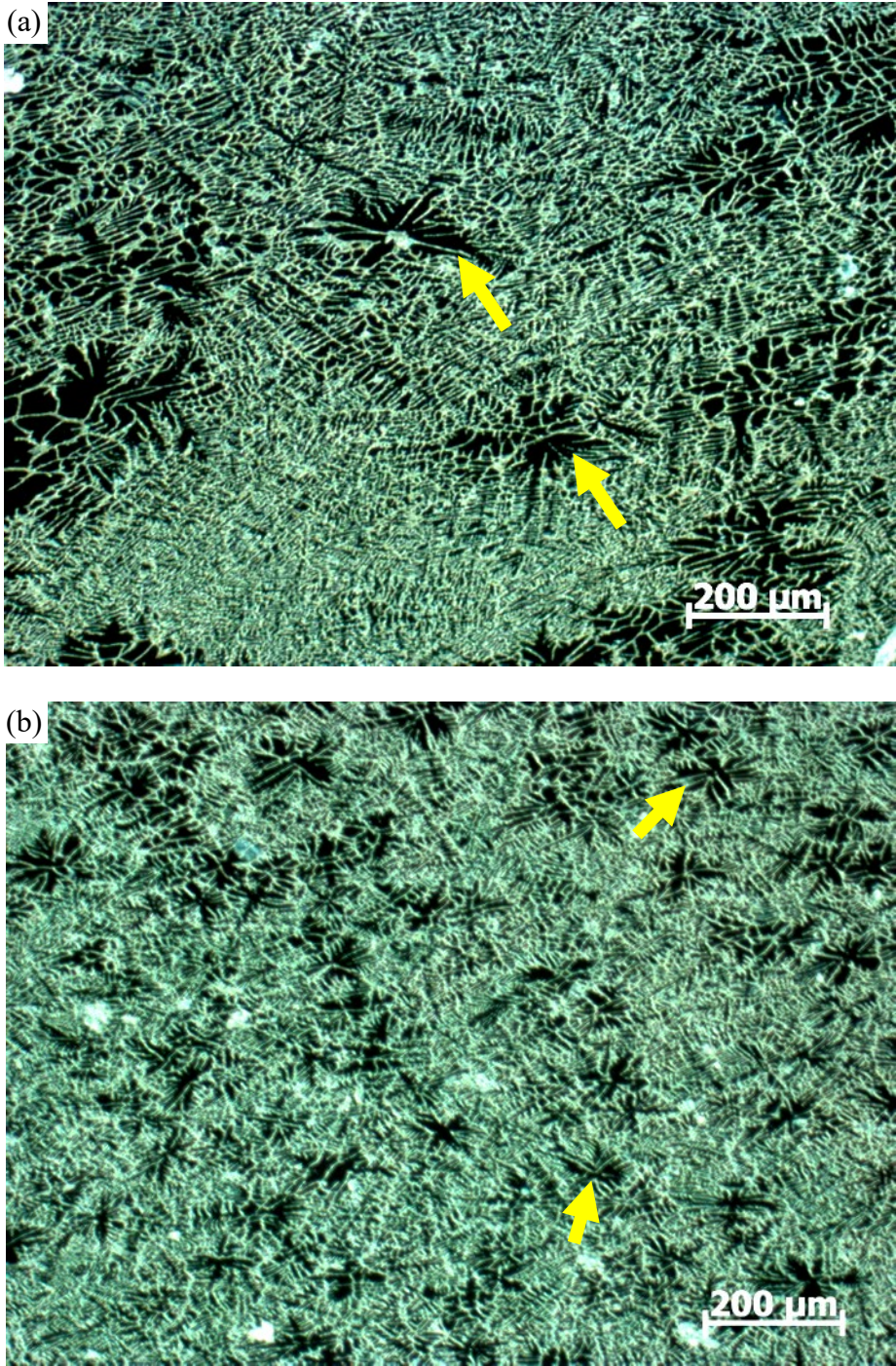
Fig. 3 Darkfield light microscope images of the anodized longitudinal direction cross-sectioned (a) IA and (b) IA+GR as-cast TRC strips. The number of coarse dendritic "floating" grains is 4 times higher in the GR strip. DAS is also finer in GR strip. Arrows indicates examples of "floating" grains. Note: inter-dendritic region are brighter in the darkfield reflected-light image.

Figure 4
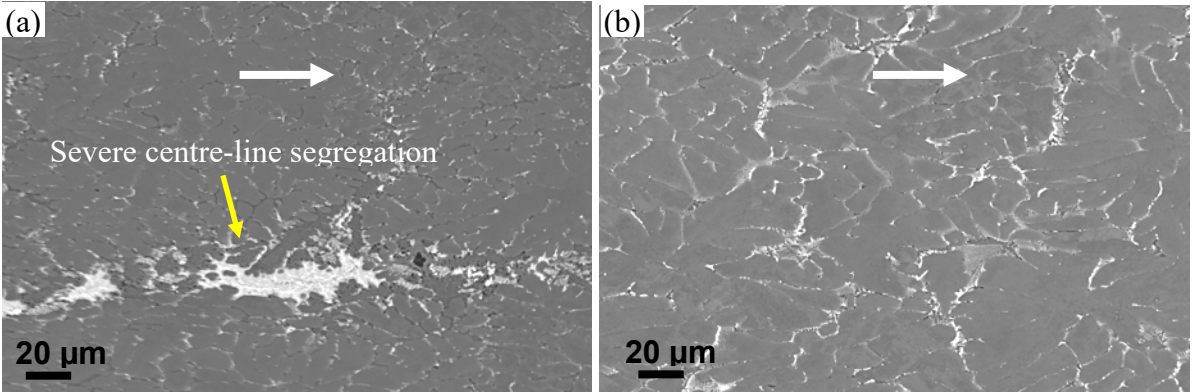
Fig. 4. Back scattered (BSE) SEM images of the longitudinal cross-sectioned (a) IA and (b) IA+GR as-cast TRC strips. Severe centre-line segregation is observed in the strip without grain refiner. Horizontal arrow shows the cast direction.

Figure 5
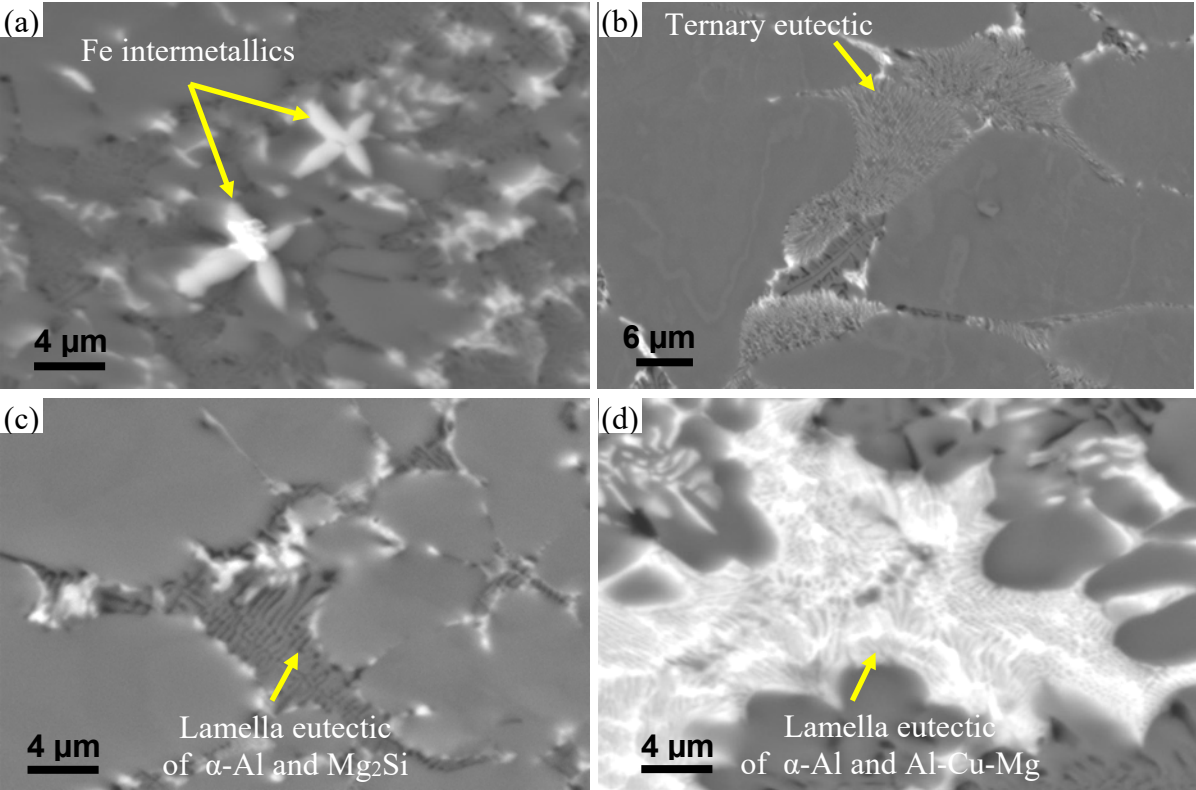
Fig. 5. High magnification BSE SEM images showing the presence of different phases at the centre-line segregation region of the IA strip cast without grain refiner. Where (a) shows the Fe bearing intermetallic, (b) ternary eutectic of α-Al, Mg_2Si and Fe bearing intermetallic, (c) lamella eutectic of α-Al and Mg_2Si, and (d) lamella eutectic of α-Al and Al-Cu-Mg phase.

Figure 6
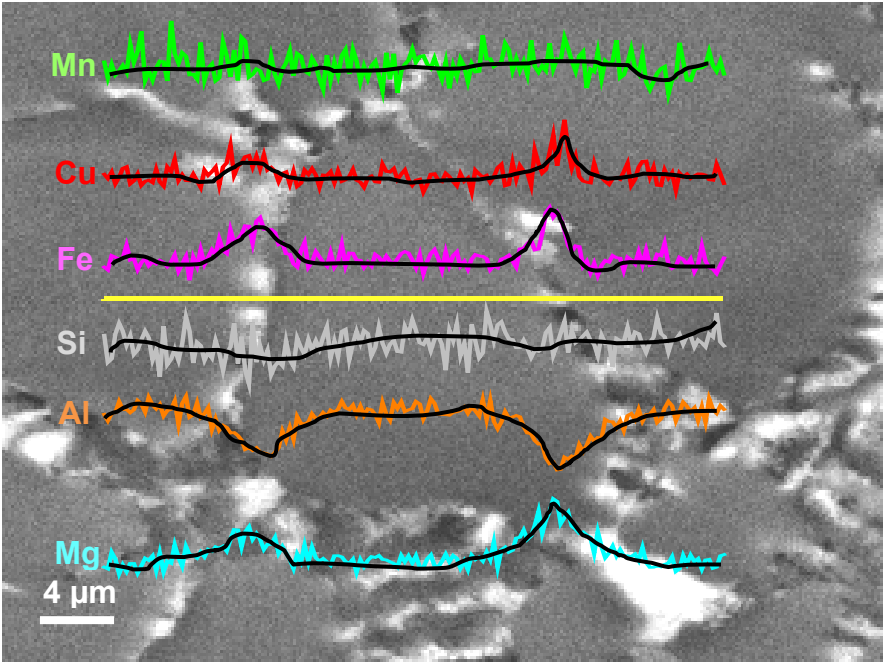
Fig. 6. Line scan (EDS) showing microsegregation of solute elements in the inter-dendritic regions.

Figure 7
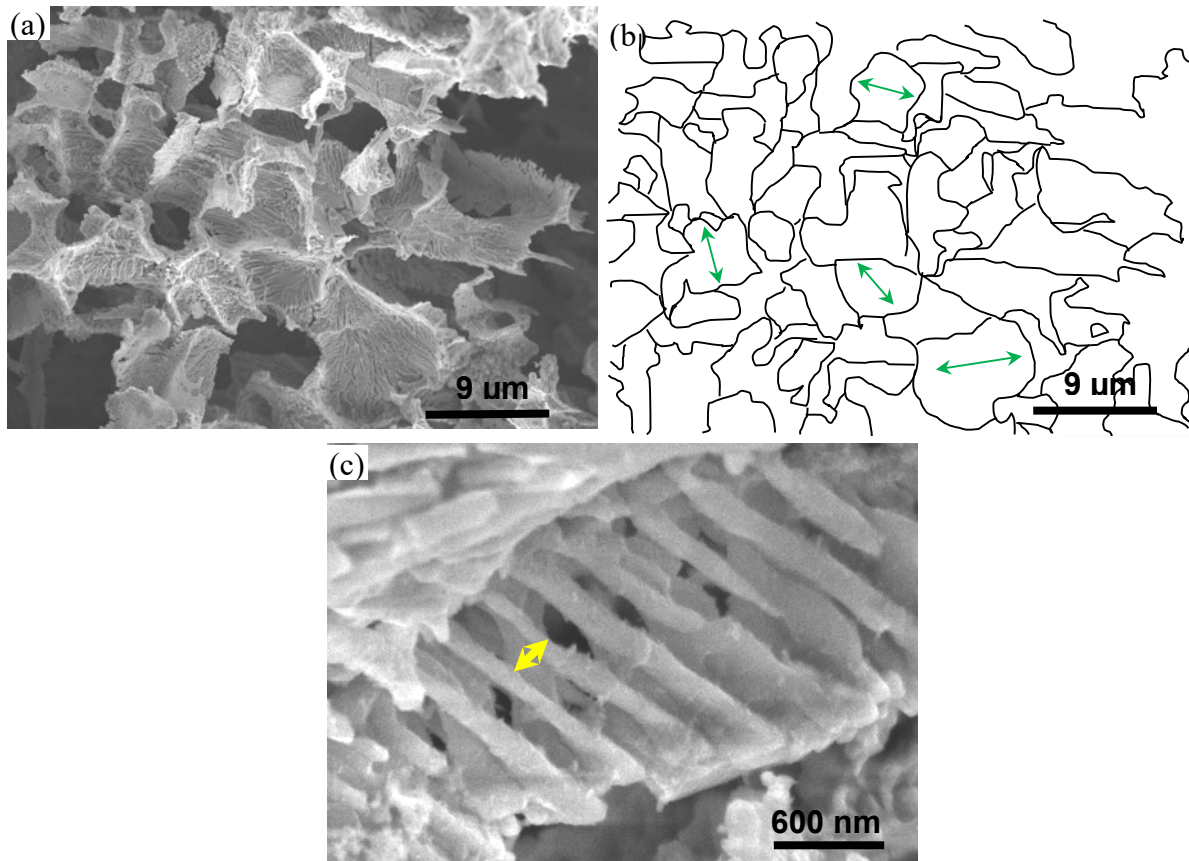
Fig. 7. 3D analysis of the IA+GR as-cast TRC strip. Secondary phase particles are well interconnected (a), and the trace diagram (b) from (a) indicating connectivity which was used to measure the approximate pore size (arrow). Most of these particles are fibrous in nature (c), with a spacing less than 100 nm.

Figure 8
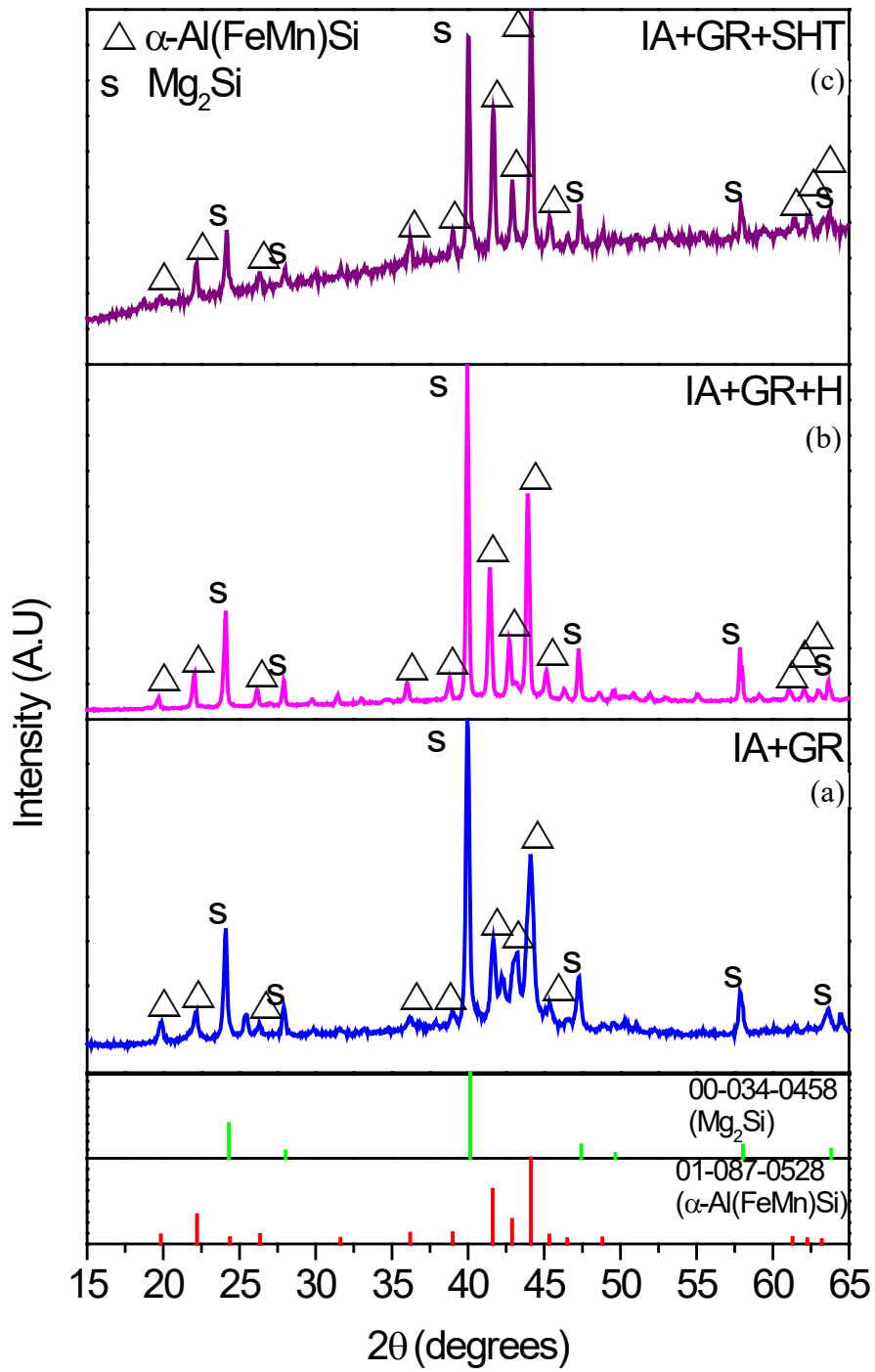
Fig. 8. XRD patterns of the extracted particles. Corresponding JCPDF file numbers used for indexing are also shown.

Figure 9
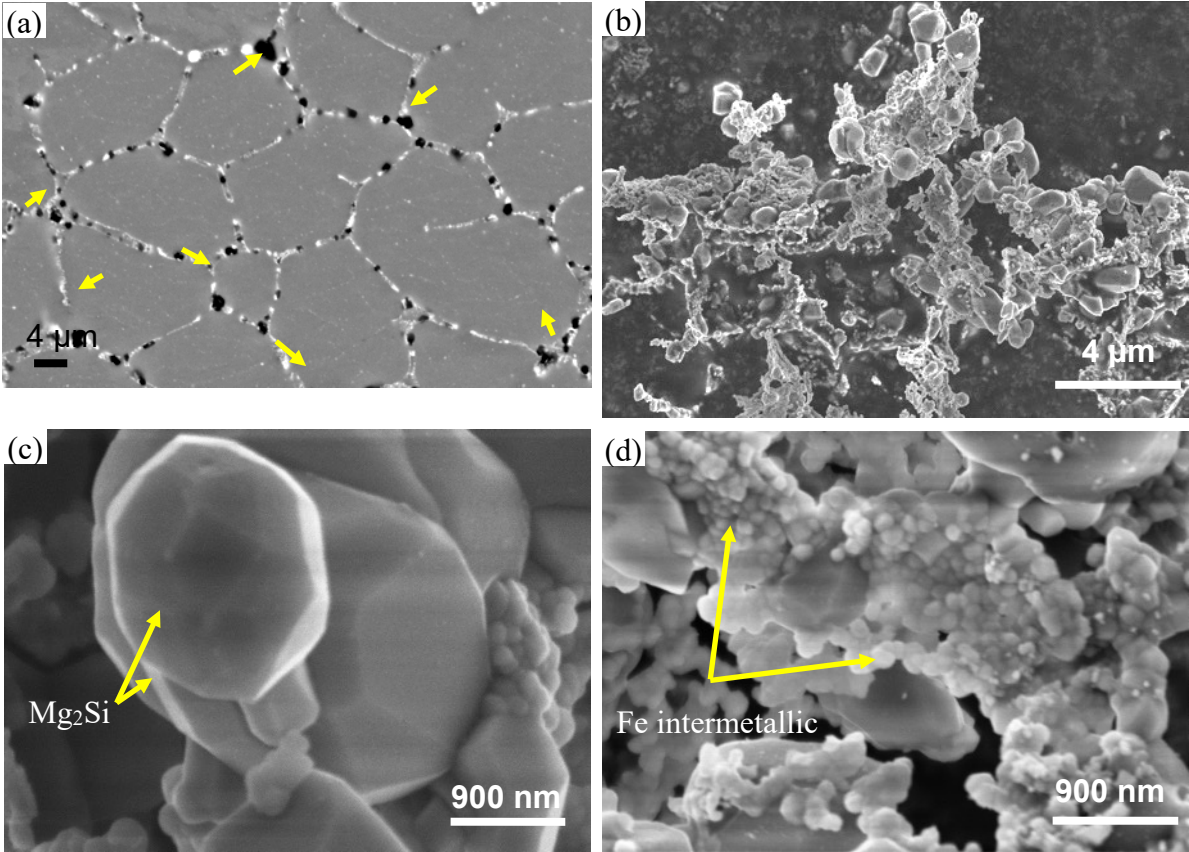
Fig. 9. 2D and 3D analysis of the homogenised IA+GR TRC strip. The transverse cross-section of homogenised strip (a) shows the cell/grain boundaries decorated with fine Fe bearing intermetallic (bright) and Mg_2Si (dark) particles. Coarse Mg_2Si (marked with arrow) was mainly observed at the triple junctions of the boundaries. 3D analysis of the extracted particles revealed (i) the absence of a dense interconnected network (b), (ii) the equiaxed Mg_2Si particles were facetted (c) and (iii) the equiaxed Fe bearing intermetallics were finer than the Mg_2Si (d).

Figure 10
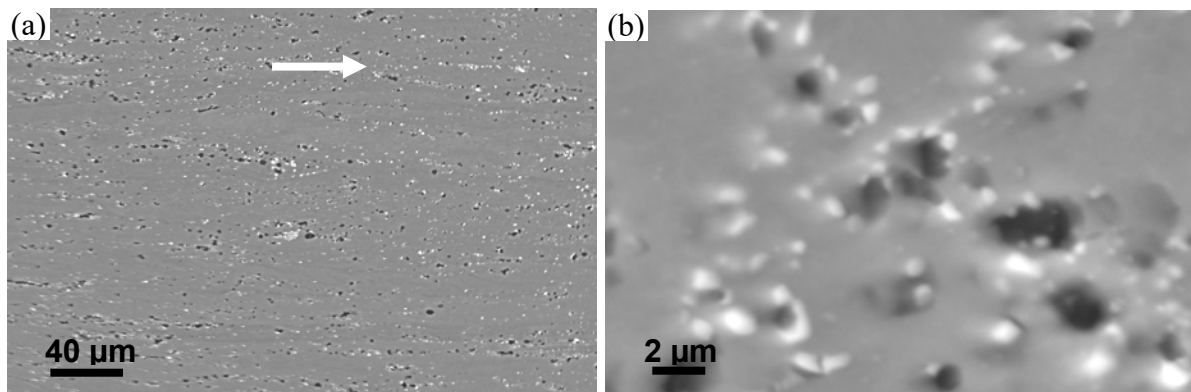
Fig. 10. BSE-SEM image of the rolled and solutionised sheet, (a) showing intermetallics aligned along the rolling direction, and (b) higher magnification of the Fe bearing intermetallics (bright particles) and Mg_2Si (dark particles). Fe bearing intermetallics are finer than the Mg_2Si.
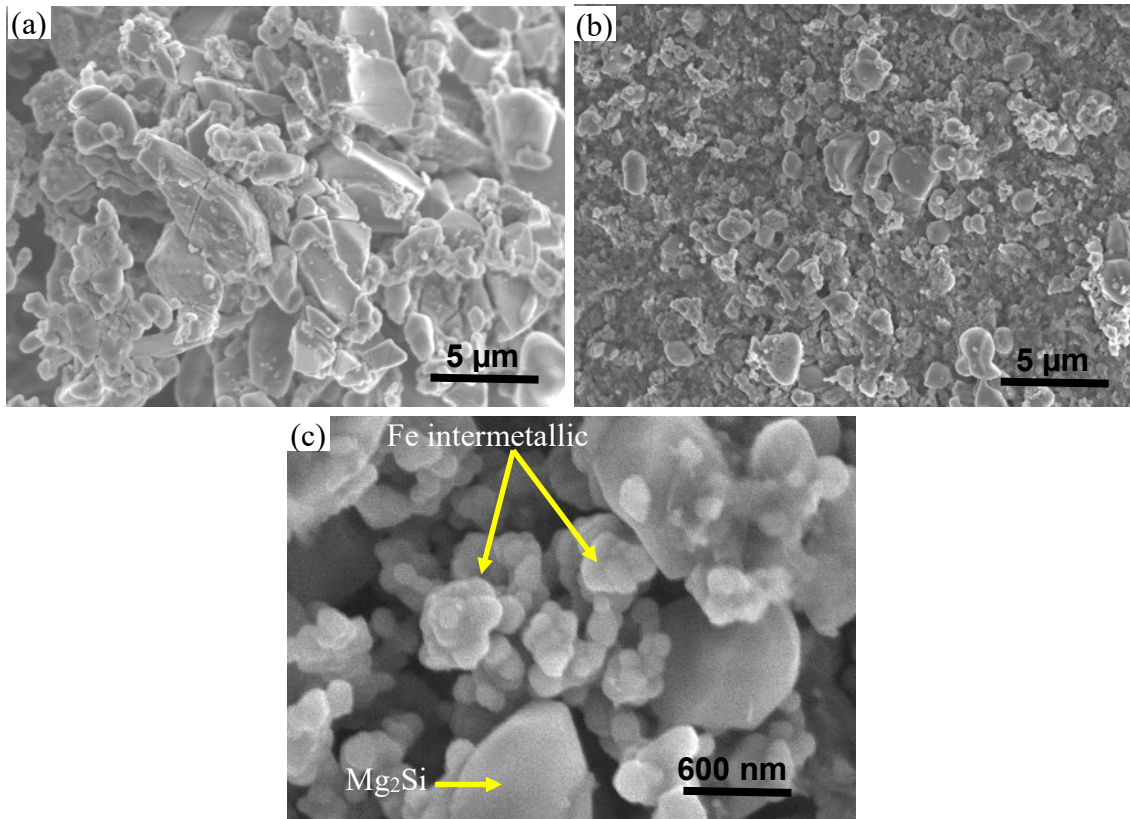
Figure 11

Fig. 11. FEG-SEM analysis of the extracted particles from the IA+GR sheets processed from (a) book mould ingot and (b,c) TRC stip. Secondary phase particles are finer in the TRC processed sheet.

Figure 12
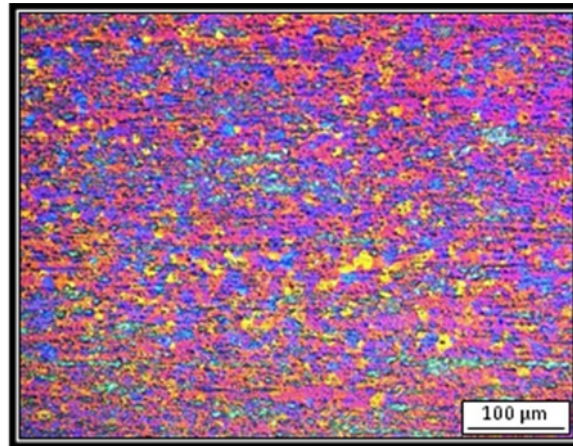
Fig. 12. Anodized microstructure of the TRC processed sheet after homogenisation, cold rolling and solution treatment.
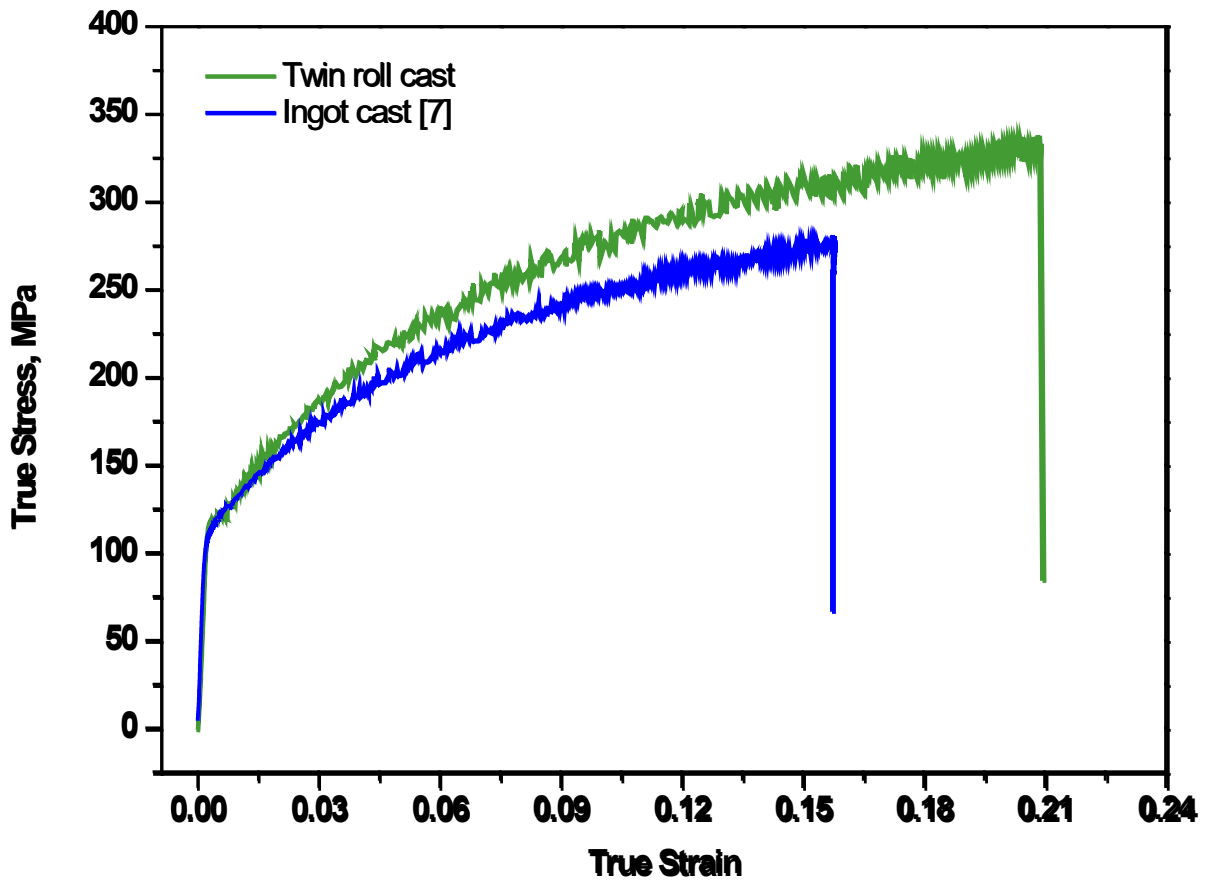
Figure 13

Fig. 13. True stress-strain curve of the sheets processed from TRC and book mould ingot casting. TRC processed sheet shows superior strength and ductility.
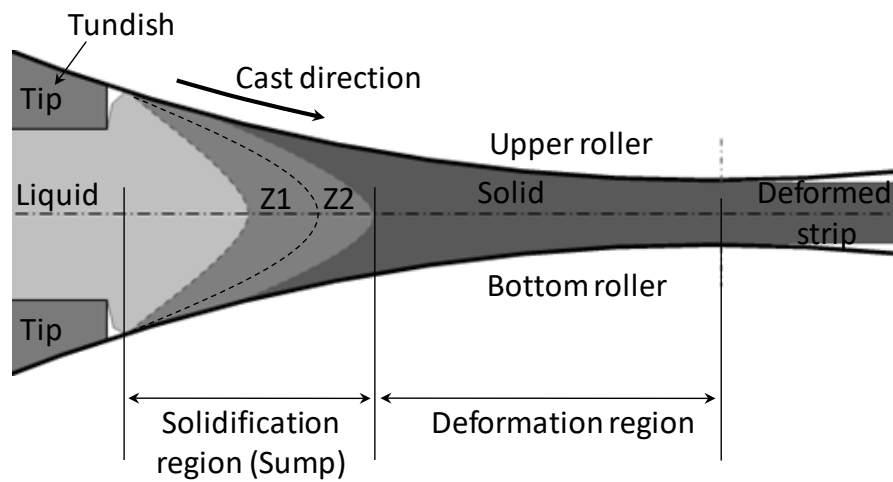
Figure 14

Fig. 14. Schematic illustration of solidification and deformation processes during TRC, where Z1 and Z2 are the slurry and mushy zones, respectively.
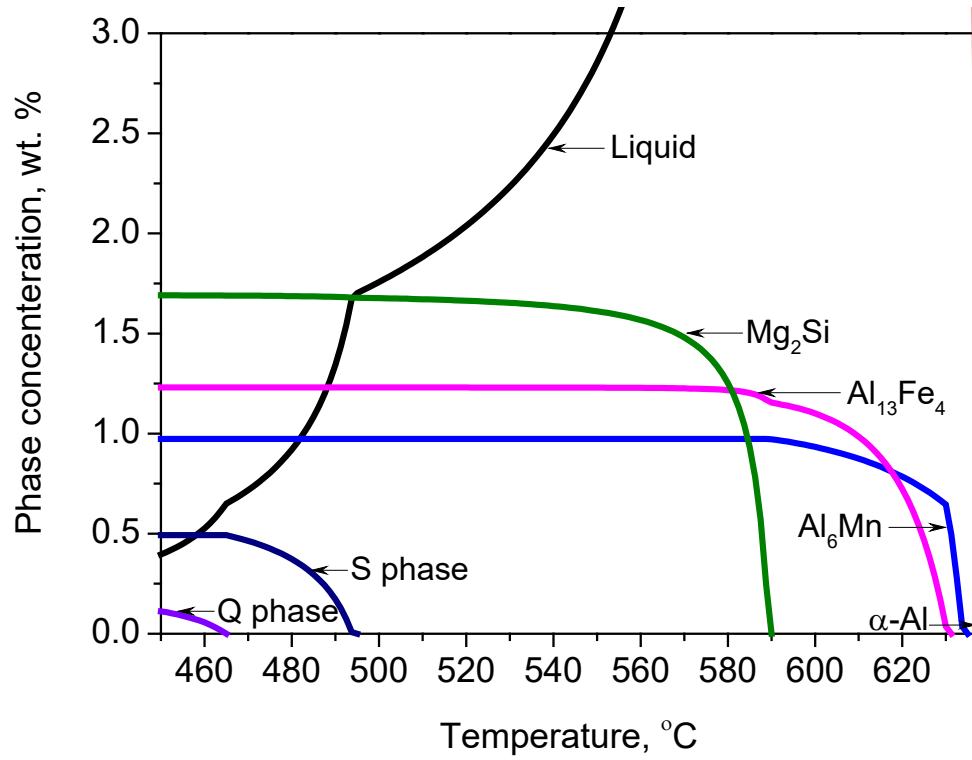
Figure 15

Fig. 15. Thermodynamic calculation of phase content in IA, under Scheil condition.
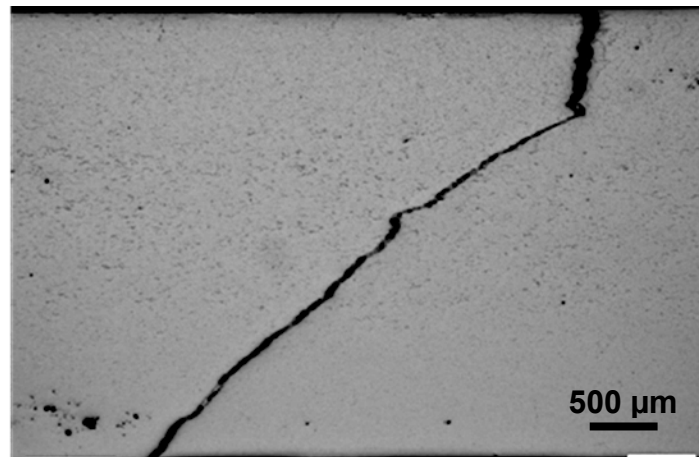
Figure 16

Fig. 16. Light microscopy image taken along the longitudinal cross-section of IA+GR TRC strip showing that fracture occurred while rolling the as-cast strip without homogenisation.